[redacted] 71967 Copy 7

463

NASA TM X-163

NASA TM X-163

[redacted]

TECHNICAL MEMORANDUM

X-163

INVESTIGATION OF MODIFICATIONS OF A TWIN-DUCT SIDE INLET UTILIZING A BOUNDARY-LAYER REMOVAL SLOT AT MACH NUMBERS FROM 1.59 TO 2.10

By Norman E. Sorensen and Thomas J. Gregory

Ames Research Center
Moffett Field, Calif.

[redacted]

[redacted]

NATIONAL AERONAUTICS AND SPACE ADMINISTRATION

WASHINGTON

September 1960

[redacted]

T

[redacted]

NATIONAL AERONAUTICS AND SPACE ADMINISTRATION

TECHNICAL MEMORANDUM X-163

INVESTIGATION OF MODIFICATIONS OF A TWIN-DUCT SIDE INLET UTILIZING A BOUNDARY-LAYER REMOVAL SLOT AT MACH NUMBERS FROM 1.59 TO 2.10*

By Norman E. Sorensen and Thomas J. Gregory

SUMMARY

A wind-tunnel investigation at Mach numbers from 1.59 to 2.10 has been made to evaluate the effects on inlet performance of several modifications to a model of a twin-duct side-inlet system with variable geometry. The modifications included providing boundary-layer removal through a slot at the inlet throat, altering the external and internal cowl and duct contours, increasing the fuselage length ahead of the inlets, and altering the height and shape of the fuselage boundary-layer diverter.

It was shown that with boundary-layer bleed through the slot, the maximum total-pressure recovery was improved about 3 to 5 percent. Computations showed that if the model was considered to be 1/8-scale the reduction in drag due to reduced initial cowl angle and frontal area of the modified cowls reduced the full-scale airplane drag about 1170 pounds for flight at Mach number 2.0 at an altitude of 35,000 feet (NASA standard day). Considerable variation in the plan-form shape of the boundary-layer diverter did not significantly alter the maximum total-pressure recovery. Unfavorable location of the inlet in the fuselage flow field prevented better performance of this twin-duct side inlet from being achieved.

INTRODUCTION

The most desirable characteristics of an air-induction system, namely, minimum drag and maximum pressure recovery, usually cannot be achieved simultaneously. Hence, most inlet designs represent a reasonable compromise of external drag and internal performance. An example of a possible compromise is contained in the experimental results reported

---

[redacted]

in reference 1. Considerable improvement in over-all system performance of an axially symmetric inlet system resulted from incorporating a rapid turn in the internal flow at the inlet throat, thereby permitting a sizable reduction in the external cowl angles and in the frontal area of the system. The reduction in external drag more than offset the small penalty in internal performance.

In another investigation (ref. 2) high pressure recovery of an inlet system was achieved through the use of a large boundary-layer bleed slot at the throat of a two-dimensional external compression inlet similar to that of the present investigation.

The foregoing results were used as a design guide in modifying the existing twin-duct side-inlet model used in reference 3. Accordingly, a wind-tunnel investigation was made to evaluate the effects on inlet performance of several modifications to a double-ramp variable-geometry configuration designed for Mach number 2.0. The modifications included providing boundary-layer removal through a slot at the inlet throat, altering the external and internal cowl contours, increasing the fuselage length ahead of the inlets which provides for more fuselage volume, and altering the height and shape of the fuselage boundary-layer diverter.

A
2
1
4

The tests were conducted in the 9- by 7-foot test section of the Ames Unitary Plan Wind Tunnel at a Reynolds number of about 2.5×10^6 per foot. The ranges of Mach number and angle of attack of the investigation were 1.59 to 2.10 and 0° to 5°, respectively.

SYMBOLS

A_c capture area of the model, 16.406 in.^{2} (sum of both inlets)

C_X external-chord-force coefficient based on capture area A_c

$C_{X_{o_{min}}}$ minimum C_X for the original cowls

h boundary-layer height

M_i local Mach number immediately ahead of the first ramp

M_∞ free-stream Mach number

m_{bl} estimated mass rate of flow through the boundary-layer bleed slots

m_3 mass rate of flow through the compressor face measured at the eight static-pressure orifices [redacted]

m_∞ mass rate of flow of free-stream air through an area equal to A_c

p_p pitot pressure measured by the boundary-layer rake

p_{t_2} total pressure at the compressor face

p_{t_∞} total pressure of the free stream

Δp total-pressure distortion parameter at the compressor face,

$$\frac{\left(p_{t_2}\right)_{max} - \left(p_{t_2}\right)_{min}}{\left(p_{t_2}\right)_{av}}$$

A
2
1
4

α angle of attack measured from the body reference axis

β angle of sideslip, positive to the left

δ_2 second ramp angle (includes first ramp angle)

Configuration Notation
(See figs. 2 and 3)

C_o original cowl

C_o' original cowl with only the outside modified to reduce the initial cowl angle and the frontal area

C_{min} cowl with the minimum frontal area and rapid internal turning of the flow

C_i cowl providing for increased boundary-layer diverter height

D_o original boundary-layer diverter

D_o' original boundary-layer diverter modified to provide for increased height

D_{cb} boundary-layer diverter with a center body

D_e extended boundary-layer diverter with the lip of the first ramp extended

D_s boundary-layer diverter with the sharp lip

G_x position of boundary-layer-bleed gate, with the subscript (x) representing the percent of maximum gate area (maximum area for both gates = 5.55 sq in.)

N_L fuselage configuration with the long nose

N_S fuselage configuration with the short nose

S slot at the throat of the inlet (area for both slots = 3.23 sq in.)

S_o no slot in the inlet

MODEL DESCRIPTION

A214

The model consisted of a fuselage forebody and twin inlets which combined into a common duct ahead of the compressor-face station. Figure 1(a) shows the model mounted on a sting in the wind tunnel; figure 1(b) shows a detail view of one of the inlets; and figures 1(c) and (d) show two of the cowls. Figure 2 is a general outline of the model and its instrumentation. Details of the cowls, slots, and fuselage boundary-layer diverters tested are shown in figure 3. A table of coordinates for the cowls is presented in table I, and the duct area distributions up to the compressor-face station are presented in figure 4.

Details of the compressor-face rake, the flow wedges for measuring the local flow direction and local Mach number immediately ahead of the first ramp of the inlet, the boundary-layer rake, and the duct internal contours are shown in figure 2. Mass flow through the main duct and through the two fuselage boundary-layer diverter ducts was regulated by movable plugs near the base of the model. Flow through the boundary-layer bleed slot (fig. 3) was regulated by a movable gate, one for each inlet, located within the fuselage. A pressure transducer was mounted in each duct to indicate the onset of instability of the main duct flow. A balance housed within the forebody measured the gross drag, and pressure orifices located in the base measured the base drag. However, for many of the configurations the balance was inoperable.

The duct contours for the range of variable second ramp angles tested are shown in figure 3. The first ramp angle was 9° for all the configurations except that used with the minimum frontal area cowl C_{min} for which a 12° first ramp angle was used. The reduced frontal area and initial angle of the modified cowl C_o' were obtained by decreasing the thickness of the original cowl C_o without changing the internal duct lines. The over-all external modification can be seen by comparing the photographs of C_o and C_o' in figures 1(c) and (d). The maximum frontal area of the

C_o cowl was reduced by about 8 percent, not including the capture area. For the cowl used with the increased boundary-layer diverter height C_i, the external and internal lines were necessarily displaced farther from the fuselage. The cowl with minimum frontal area C_{min} was obtained by recontouring the internal and external lines of the cowl and the initial portion of the subsonic diffuser. This allowed the outside of the cowl to be faired straight back, producing about a 50-percent reduction of frontal area over that of the C_o cowl. In addition, rapid internal turning of the flow resulted. The internal area distribution for all the cowls remained fixed.

TEST METHODS

The total-pressure recovery was obtained by the area weighted method using the rake at the compressor face. The main duct mass flow was obtained by the "choked plug" method using the eight static-pressure orifices ahead of the plug (see fig. 2), the known ratio of the minimum area at the plug and the area at the eight static orifices, and a flow coefficient of 0.99. The external-chord-force coefficient C_X is the chordwise component of the external forces presented in coefficient form which excludes the base pressure forces and the internal force developed by the change in momentum of the main duct flow between the free stream and the location of the eight static-pressure orifices. Also excluded from C_X is the internal force developed by the change in momentum of both the diverter duct flows. The coefficient C_X includes the internal force developed by the bleed flow through the slots since no attempt was made to measure the momentum change. The instrumentation used to measure bleed flow rates proved to be inadequate; hence, bleed flow rates for the supercritical range have been estimated as the difference between the main duct mass flow with zero bleed flow and that at maximum recovery for the various bleed flow gate settings.

The average Mach number, M_i, in a plane just ahead of the inlet was obtained with the 12^o flow wedges shown in figure 2 by means of average values of the static and total pressures. Pitot-pressure profiles of the fuselage boundary layer at this same station were obtained with the boundary-layer rake shown in figure 2.

RESULTS AND DISCUSSION

A summary table showing the configurations tested and the range of variables investigated for each configuration has been prepared and is presented as table II. The experimental results of the investigation are presented in figures 5 to 11 and in table III.

[redacted]

Effects of Boundary-Layer Bleed and Angle of Attack

The effects of boundary-layer bleed at the throat of the inlet are considered for the model configuration which involved variation in the length of the fuselage forebody and changes in both the height of the fuselage boundary-layer diverter and the accompanying cowl shape. Data are presented in figures 5(a), (b), (c), and (d), and summarized in figure 5(e) for Mach number 2.0. Also shown in figure 5(e) is the maximum recovery for the original inlet-fuselage combination without any provision for boundary-layer bleed at the throat. Generally a significant improvement in peak pressure recovery above that of the original inlet results from throat bleed and configuration changes, the peak recoveries being about 3 to 5 percent greater. Extending the fuselage forebody ahead of the inlet results in such a large increase in boundary-layer thickness that considerable low-energy air is spilled over the diverter on to the compression surfaces and into the inlet (see fig. 6). Without bleed the recovery is below that of the basic configuration without a slot. With bleed the peak recovery is approximately 1-1/2 percent greater than that of the short nose configuration, but more bleed is required to achieve the peak recovery. When the diverter height is increased to avoid injestion of some of the fuselage boundary layer, the recovery with zero bleed is increased above that of the short nose configuration, and the maximum recovery for this configuration is achieved at a bleed flow rate comparable to the bleed requirements for the short nose configuration. The net result is that the maximum recovery with or without bleed for the long nose configuration was greater than that for the short nose. The reason for this lies in the effect of the fuselage flow field ahead of the inlet, which will be discussed later in more detail.

In general, the performance of this type of side inlet at angle of attack is known to be relatively poor as a result of crossflow effects from the fuselage ahead of the inlet. The fuselage forebody at angle of attack not only has a boundary-layer build-up in the axial direction, but also in the crossflow direction along the sides. If the fuselage boundary-layer diverter is not high enough to accommodate the additional crossflow boundary layer, the inlet performance suffers accordingly. These effects are indicated by figure 5(e) wherein the maximum pressure recovery is plotted as a function of angle of attack and by the corresponding boundary-layer profiles of figure 6. Obviously at 5° angle of attack, extending the forebody with its attendant increase in boundary-layer thickness without increasing the diverter height is disastrous and results in a loss of 12-percent pressure recovery.

[redacted]

Effect of Variable Geometry

If an inlet-duct combination is to maintain high performance over a wide range of Mach numbers, provision for variation of the geometry of the ramp angles, together with the minimum throat area, must be made. In the case of the present inlet, the first-ramp angle was fixed and only the second-ramp angle and minimum throat area were variable (see fig. 3). The critical nature of the second-ramp angle at high free-stream Mach number is shown in figure 7, wherein the maximum total-pressure recovery is plotted as a function of the second-ramp angle for the free-stream Mach numbers indicated. This figure is a cross plot of the data appearing in table III. It is evident that the maximum recovery becomes more sensitive to change in second-ramp angle as the free-stream Mach number is increased.

Effect of Fuselage Flow Field

A comparison of the experimental peak total-pressure recovery with the theoretical shock recovery may indicate if there is a loss in recovery associated with induced effects. In the present case the inlet is located in such a position that the average Mach number at the inlet is greater than the free-stream Mach number (see fig. 6). As a result, the shock, boundary layer, and other possible losses are greater than they would be if the Mach number at the inlet were equal to the free-stream value. An estimate of the magnitude of the total-pressure recovery loss is shown in figure 8. The curve of peak recovery is cross-plotted from figure 7 for each configuration. The theoretical three-shock recovery calculated from reference 4 is compared with the optimum pressure recovery from figure 7 which does not include subsonic diffuser losses. The estimated recovery with the inlet Mach number equal to the free-stream Mach number is obtained with the aid of figure 6. For example, for the short nose configuration, at $M_\infty = 2.0$ and $\alpha = 2.1^\circ$, find M_i to be 2.12 from figure 6. Enter figure 8 at $M_i = 2.12$ and note that the change in measured peak recovery between M_∞ and M_i is about 0.036. Add this recovery to the measured recovery (0.862) at $M_\infty = 2.0$ to find the estimated recovery (0.898). An improvement of 2 to 4 percent is shown for all three configurations. This indicates that substantial increases in recovery would be possible if the inlet were located in a more favorable fuselage flow field.

Effect of Boundary-Layer Diverters

Several possible boundary-layer diverters were tested to assess the effects of the diverter on the inlet performance since it is known that

[redacted]

the diverter can have an effect on the upstream boundary layer. Figure 9 shows the results at $M_\infty = 2.00$ and $\alpha = 2.1^\circ$ for the four boundary-layer diverter configurations illustrated in figure 3. The diverter with the first-ramp-lip extension D_e causes a significant loss in total-pressure recovery, probably because of the boundary-layer build-up on the extension. The other three diverter configurations produce little change in these parameters, indicating considerable freedom in the design of the diverter plan form.

Effects of Cowl Modifications and Rapid Turning

A high pressure field acting on the frontal area of the cowl of an inlet is always a potential source of excessive external drag. Obviously, reducing the frontal area and the initial external cowl angle reduces the drag. A minimum frontal area, however, can be attained only through the incorporation of rapid turning of the internal flow. The experimental increments of drag reduction attainable by reducing the frontal area and initial cowl angle are shown in figure 10. The cowl with only the outside contours modified C_o' (see fig. 3) and with no bleed slot S_o shows about a 0.12 reduction in minimum external-chord-force coefficient from that of the original cowl. Considering the model to be 1/8-scale then in terms of drag on a full-scale airplane ($M_\infty = 2.00$, altitude = 35,000 feet, NASA standard day) this amounts to about 1170 pounds. The cowl with minimum frontal area and rapid turning of the flow at the throat C_{min} and with a bleed slot S similarly has a drag reduction which is probably greater than shown because no account is made in the experimental drag for the internal momentum loss of the bleed mass flow. This reduction in drag was realized with little change in maximum total-pressure recovery. (Compare the maximum recovery data point here of 0.865 with the peak recovery of 0.867 shown in figure 5(e) for the short nose configuration.) Insofar as stable mass-flow range is concerned, although the minimum stable mass flow is not well defined here for the C_{min} configuration, data available at other angles of attack indicate little change from that of the other two configurations.

Distortion Contours

Figure 11 shows typical total-pressure contours at the compressor face for the three main configurations previously discussed. The plots are for peak total-pressure recovery points at Mach number 2.00 and angles of attack of 0.1°, 2.1°, and 5.1°. In addition, for one of the long nose configurations, there are contours for five bleed flow rates at $\alpha = 2.1^\circ$.

[redacted]

The improvement in the uniformity of the contours with the initial increases of bleed is apparent as is the reduction of recovery in the lower portion of the duct with increasing angle of attack.[1]

SUMMARY OF RESULTS

It has been shown that with boundary-layer bleed through a slot at the throat of the inlet and with configuration changes the maximum total-pressure recovery was improved by about 3 to 5 percent over that of a similar configuration without a slot. In addition, if the model was considered to be 1/8-scale, reducing the initial cowl angle and the frontal area of the cowl by changing only the outside contours of the original configuration would reduce the full-scale airplane drag by about 1170 pounds (M_∞ = 2.00, altitude = 35,000 feet, NASA standard day). Recontouring the internal and external lines of the cowls to further reduce the frontal area resulted in internal duct lines which produced rapid turning of the internal flow. For this latter modification, the drag reduction was probably even greater. It was noted that the total-pressure recovery need not be reduced by rapid turning of the flow if the boundary layer at the throat of the inlet is controlled with a bleed slot. Unfavorable location of the inlet in the fuselage flow field prevented better performance of this twin-duct side inlet from being achieved. It was also shown that considerable variation in the plan-form shape of the boundary-layer diverter did not significantly alter the maximum total-pressure recovery.

A
2
1
4

Ames Research Center
National Aeronautics and Space Administration
Moffett Field, Calif., Nov. 17, 1959

---

[1]The bleed mass-flow ratio is not available for $\alpha = 0.1^\circ$ and 5.1°, but the ratio is believed to be relatively unaffected by these changes in angle of attack.

[redacted]

REFERENCES

1. Connors, James F., Wise, George A., and Lovell, Calvin J.: Investigation of Translating-Double-Cone Axisymmetric Inlets With Cowl Projected Areas 40 and 20 Percent of Maximum at Mach Numbers From 3.0 to 2.0. NACA RM E57C06, 1957.

2. Vargo, Donald J., Parks, Phillip N., and Davis, Owen H.: Investigation of a High-Performance Top Inlet to Mach Number of 2.0 and at Angles of Attack to 20°. NACA RM E57A21, 1957.

3. Yeager, Richard A., Beheim, Milton A., and Klann, John L.: Performance of Twin-Duct Variable-Geometry Side Inlets at Mach Numbers of 1.5 to 2.0. NACA RM E56K15, 1957.

4. Ames Research Staff: Equations, Tables, and Charts for Compressible Flow. NACA Rep. 1135, 1953.

[redacted]

[redacted]

TABLE I.- DUCT AND COWL CENTER-LINE COORDINATES

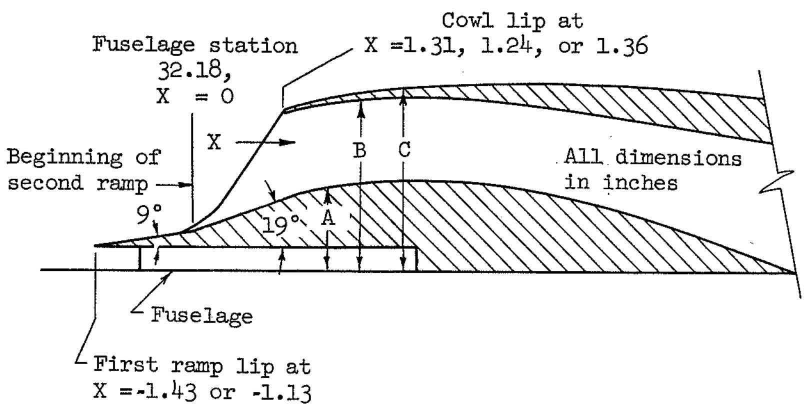

X	C_o		
	A	B	C
-1.43	0.34	----	----
0	.57	----	----
1.31	----	2.34	2.34
1.40	----	2.34	2.43
1.63	1.13	2.40	2.53
1.80	1.18	2.45	2.60
2.00	1.22	2.48	2.65
2.20	1.25	2.51	2.70
2.40	1.27	2.52	2.73
2.60	1.28	2.54	2.76
2.80	1.29	2.55	2.78
3.00	1.29	2.55	2.80
3.20	1.29	2.56	2.81
3.40	1.28	2.54	2.81
3.60	1.27	2.53	2.82
3.80	1.24	2.52	2.82
4.00	1.22	2.51	2.82
4.20	1.20	2.50	2.82
4.40	1.17	2.48	2.81
4.60	1.13	2.47	2.80
4.80	1.10	2.44	2.80
5.00	1.07	2.42	2.79
5.20	1.02	2.40	2.78
5.60	0.93	2.36	2.75
6.00	.84	2.30	2.72
6.40	.73	2.25	2.70
6.80	.63	2.18	2.68
7.20	.52	2.11	2.65
7.60	.40	2.04	2.62
8.00	.29	1.98	2.61
8.40	.17	1.90	2.60
8.80	.05	1.82	2.59
9.32	- .11	1.72	2.59

X	C_o'		
	A	B	C
-1.43	0.34	----	----
0	.57	----	----
1.24	----	2.34	2.34
1.40	----	2.37	2.43
1.63	1.13	2.42	2.48
Same as C_o	Same as C_o	Same as C_o	2.53
			2.58
			2.62
			2.65
			2.68
			2.70
			2.72
			2.74
			2.75
			2.76
			2.77
			2.78
			2.78
			2.78
			2.78
			2.77
			2.77
			2.76
			2.73
			2.71
			2.69
			2.68
			2.65
			2.62
			2.61
			2.60
			2.59
			2.59

X	C_{min}		
	A	B	C
-1.13	0.34	----	----
0	.57	----	----
1.24	----	2.34	2.34
1.40	----	2.37	2.42
1.63	1.13	2.41	2.48
Same as C_o	1.18	2.43	2.51
	1.20	2.45	2.54
	1.22	2.45	2.56
	1.23	2.46	2.58
	1.23	2.46	
	1.23	2.45	
	1.22	2.44	
	1.22	2.44	
	1.21	2.43	
	1.20	2.43	
	1.19	2.42	
	1.18	2.41	
	1.17	2.40	
	1.15	2.40	
	1.13	2.39	
	1.12	2.38	
	1.10	2.36	
	1.08	2.34	
	1.03	2.31	
	0.96	2.28	
	.87	2.22	
	.76	2.18	
	.63	2.12	
	.50	2.06	
	.36	1.99	
	.22	1.92	2.58
	.08	1.84	2.59
	- .11	1.72	2.59

X	C_i		
	A	B	C
-1.43	0.59	----	----
0	.82	----	----
1.36	----	2.59	2.59
1.40	----	2.58	2.65
1.63	1.38	2.63	2.71
Same as C_o	1.44	2.68	2.76
	1.48	2.72	2.81
	1.51	2.75	2.85
	1.53	2.78	2.88
	1.54	2.80	2.91
	1.55	2.81	2.93
	1.55	2.82	2.95
	1.54	2.82	2.97
	1.53	2.82	2.97
	1.52	2.81	2.98
	1.49	2.80	2.98
	1.47	2.78	2.98
	1.43	2.75	2.97
	1.40	2.72	2.96
	1.37	2.70	2.94
	1.32	2.68	2.92
	1.28	2.63	2.91
	1.24	2.60	2.89
	1.14	2.53	2.85
	1.03	2.45	2.80
	0.92	2.37	2.76
	.80	2.28	2.72
	.67	2.18	2.69
	.54	2.09	2.66
	.40	2.00	2.63
	.25	1.91	2.61
	.10	1.82	2.59
	- .11	1.72	2.59

[redacted]

[redacted]

TABLE II.- SUMMARY OF THE TEST

Source	Configuration	Second-ramp angle, deg	Bleed gate position, G_x, percent	Free-stream Mach number, M_∞	Angle of attack, α, deg
Fig. 5(a)	$N_SC_o'D_oS$	19	0-100	2.00	2.1
Fig. 5(b)	$N_LC_o'D_oS$	19	0-100	2.00	2.1
Fig. 5(c)	$N_LC_iD_o'S$	19	0-72	2.00	2.1
Fig. 5(d)	$N_SC_o'D_oS$ $N_LC_o'D_oS$ $N_LC_iD_o'S$	19 19 19	50 50 50	2.00 2.00 2.00	0.1, 2.1, 5.1 0.1, 2.1, 5.1 0.1, 2.1, 5.1
Table III	$N_SC_o'D_oS$	8, 13, 19, 30	50	1.59, 1.70 1.90, 2.00 2.10	2.1
Table III	$N_LC_oD_oS$	8, 10, 13, 17, 19, 23, 30	50	1.59, 1.70, 1.90, 2.00, 2.10	2.1
Table III	$N_LC_iD_o'S$	10, 13, 19	50	1.59, 1.70, 1.90, 2.00, 2.10	2.1
Fig. 9	$N_SC_o'D_oS_o$ $N_SC_o'D_sS_o$ $N_SC_o'D_{cb}S_o$ $N_SC_o'D_eS_o$	19 19 19 19	-- -- -- --	2.00 2.00 2.00 2.00	2.1 2.1 2.1 2.1
Fig. 10	$N_SC_oD_oS_o$ $N_SC_o'D_oS_o$ $N_SC_{min}D_oS$	19 19 19	-- -- Unknown	2.00 2.00 2.00	2.1 2.1 2.1

A
2
1
4

[redacted]

TABLE III.- EXPERIMENTAL DATA FOR VARIABLE GEOMETRY; $\alpha = 2.1^{\circ}$

(a) $N_S C_o ' D_o S G_{50}$

p_{t_2}/p_{t_∞}	m_3/m_∞	p_{t_2}/p_{t_∞}	m_3/m_∞	p_{t_2}/p_{t_∞}	m_3/m_∞	p_{t_2}/p_{t_∞}	m_3/m_∞
$M_\infty = 1.59;\ \delta_2 = 8^{\circ}$		$M_\infty = 1.59;\ \delta_2 = 13^{\circ}$		$M_\infty = 1.70;\ \delta_2 = 19^{\circ}$		$M_\infty = 1.59;\ \delta_2 = 30^{\circ}$	
0.862	0.485	0.875	0.474	0.859	0.490	0.899	0.261
.852	.494	.875	.500	.937	.542	.935	.296
.874	.561	.896	.531	.938	.579	.936	.328
.906	.620	.955	.582	.938	.617	.932	.369
.950	.701	.952	.628	.897	.644	.919	.407
.948	.736	.949	.682	.937	.666	.903	.426
.927	.771	.949	.708	.928	.686	.864	.444
.901	.811	.945	.751	.897	.708	.801	.460
.874	.833	.933	.780	.859	.722		
		.907	.799	.862	.725		
$M_\infty = 1.70;\ \delta_2 = 8^{\circ}$		$M_\infty = 1.70;\ \delta_2 = 13^{\circ}$		$M_\infty = 1.90;\ \delta_2 = 19^{\circ}$		$M_\infty = 1.70;\ \delta_2 = 30^{\circ}$	
.802	.518	.868	.587	.830	.628	.858	0.310
.803	.642	.938	.649	.892	.681	.899	.344
.881	.711	.933	.677	.885	.703	.909	.388
.912	.778	.928	.719	.886	.731	.898	.427
.887	.798	.931	.719	.885	.758	.879	.447
.859	.829	.930	.719	.850	.775	.842	.467
.829	.853	.928	.749	.813	.793	.775	.480
.795	.855	.902	.812				
$M_\infty = 1.90;\ \delta_2 = 8^{\circ}$		$M_\infty = 1.90;\ \delta_2 = 13^{\circ}$		$M_\infty = 2.00;\ \delta_2 = 19^{\circ}$		$M_\infty = 1.90;\ \delta_2 = 30^{\circ}$	
.759	.706	.867	.753	.759	.626	.790	.386
.783	.762	.859	.774	.854	.727	.855	.428
.805	.804	.849	.795	.851	.744	.856	.472
.778	.813	.836	.831	.851	.745	.833	.492
.729	.858	.799	.834	.852	.746	.793	.509
.767	.860			.837	.799	.730	.524
.697	.870			.813	.809		
				.778	.826		
				.860	.904		
$M_\infty = 2.00;\ \delta_2 = 8^{\circ}$		$M_\infty = 2.00;\ \delta_2 = 13^{\circ}$		$M_\infty = 2.10;\ \delta_2 = 19^{\circ}$		$M_\infty = 2.00;\ \delta_2 = 30^{\circ}$	
.726	.773	.784	.754	.744	.683	.735	.412
.753	.826	.814	.797	.809	.755	.829	.476
.739	.841	.800	.815	.816	.779	.830	.499
.720	.879	.786	.849	.826	.804	.809	.518
.686	.879	.751	.851	.803	.815	.768	.535
.656	.894			.768	.832		
.632	.898			.736	.849		

[redacted]

TABLE III.- EXPERIMENTAL DATA FOR VARIABLE GEOMETRY; $\alpha = 2.1^{\circ}$ - Continued

(b) $N_LC_O'D_OSG_{50}$

p_{t_2}/p_{t_∞}	m_3/m_∞	p_{t_2}/p_{t_∞}	m_3/m_∞	p_{t_2}/p_{t_∞}	m_3/m_∞	p_{t_2}/p_{t_∞}	m_3/m_∞
$M_\infty = 1.59$; $\delta_2 = 8^{\circ}$		$M_\infty = 1.59$; $\delta_2 = 10^{\circ}$		$M_\infty = 1.59$; $\delta_2 = 13^{\circ}$		$M_\infty = 1.59$; $\delta_2 = 17^{\circ}$	
0.891	0.652	0.860	0.536	0.912	0.623	0.916	0.553
.933	.740	.879	.600	.948	.670	.949	.593
.935	.747	.945	.713	.948	.678	.950	.609
.937	.754	.944	.732	.941	.731	.951	.610
.927	.804	.944	.733	.919	.762	.946	.645
.898	.811	.943	.733	.881	.785	.924	.690
.870	.833	.938	.749			.883	.713
		.932	.764				
		.915	.793				
		.896	.810				
$M_\infty = 1.70$; $\delta_2 = 8^{\circ}$		$M_\infty = 1.70$; $\delta_2 = 10^{\circ}$		$M_\infty = 1.70$; $\delta_2 = 13^{\circ}$		$M_\infty = 1.70$; $\delta_2 = 17^{\circ}$	
.861	.725	.901	.756	.919	.709	.913	.644
.895	.740	.915	.775	.932	.742	.937	.669
.891	.802	.909	.787	.931	.752	.939	.678
.868	.815	.915	.775	.922	.775	.929	.715
.843	.843	.896	.795	.896	.801	.889	.744
		.876	.820	.857	.824	.841	.755
		.853	.831				
$M_\infty = 1.90$; $\delta_2 = 8^{\circ}$		$M_\infty = 1.90$; $\delta_2 = 10^{\circ}$		$M_\infty = 1.90$; $\delta_2 = 13^{\circ}$		$M_\infty = 1.90$; $\delta_2 = 17^{\circ}$	
.749	.782	.802	.788	.802	.722	.858	.708
.778	.786	.811	.811	.859	.791	.897	.745
.778	.790	.805	.825	.853	.799	.892	.772
.795	.794	.754	.849	.821	.829	.857	.798
.780	.812	.785	.852	.780	.841	.812	.817
		.725	.856	.739	.851	.763	.829
$M_\infty = 2.00$; $\delta_2 = 8^{\circ}$		$M_\infty = 2.00$; $\delta_2 = 10^{\circ}$		$M_\infty = 2.00$; $\delta_2 = 13^{\circ}$		$M_\infty = 2.00$; $\delta_2 = 17^{\circ}$	
.737	.799	.739	.796	.769	.765	.796	.717
.733	.820	.765	.841	.775	.821	.862	.790
.745	.840	.762	.851	.803	.835	.851	.809
.742	.846	.707	.864	.749	.846	.817	.829
.705	.850	.737	.868	.702	.861	.773	.847
.671	.886	.681	.873	.664	.874	.728	.865

[redacted]

[redacted]

TABLE III.- EXPERIMENTAL DATA FOR VARIABLE GEOMETRY;
$\alpha = 2.1^\circ$ - Continued
(b) $N_L C_o{}' D_o S G_{50}$ - Concluded

A
2
1
4

p_{t_2}/p_{t_∞}	m_3/m_∞	p_{t_2}/p_{t_∞}	m_3/m_∞	p_{t_2}/p_{t_∞}	m_3/m_∞
$M_\infty = 1.59$; $\delta_2 = 19^\circ$		$M_\infty = 1.59$; $\delta_2 = 23^\circ$		$M_\infty = 1.59$; $\delta_2 = 30^\circ$	
0.898	0.507	0.869	0.421	0.900	0.333
.929	.547	.919	.467	.908	.345
.944	.567	.929	.491	.912	.358
.939	.619	.929	.502	.896	.395
.909	.652	.915	.549	.869	.415
.867	.675	.925	.550	.818	.445
.815	.678	.887	.572		
		.853	.587		
$M_\infty = 1.70$; $\delta_2 = 19^\circ$		$M_\infty = 1.70$; $\delta_2 = 23^\circ$		$M_\infty = 1.70$; $\delta_2 = 30^\circ$	
.925	.626	.873	.514	.850	.368
.933	.648	.908	.546	.873	.387
.931	.664	.907	.572	.873	.425
.851	.715	.896	.590	.844	.439
.800	.720	.881	.599	.790	.464
.896	.848	.844	.611	.722	.471
.897	.887	.805	.624		
$M_\infty = 1.90$; $\delta_2 = 19^\circ$		$M_\infty = 1.90$; $\delta_2 = 23^\circ$		$M_\infty = 1.90$; $\delta_2 = 30^\circ$	
.872	.675	.805	.571	.786	.431
.904	.724	.876	.640	.812	.464
.898	.742	.865	.656	.804	.473
.757	.771	.845	.662	.766	.491
.807	.787	.821	.675	.708	.510
.888	.799	.781	.682		
.854	.978	.740	.691		
$M_\infty = 2.00$; $\delta_2 = 19^\circ$		$M_\infty = 2.00$; $\delta_2 = 23^\circ$		$M_\infty = 2.00$; $\delta_2 = 30^\circ$	
.811	.693	.769	.604	.763	.472
.872	.765	.850	.690	.776	.489
.865	.774	.837	.696	.775	.495
.856	.783	.800	.705	.740	.515
.845	.788	.759	.729	.681	.528
.809	.803	.720	.737		
.774	.819				
$M_\infty = 2.10$; $\delta_2 = 19^\circ$					
.792	.731				
.821	.805				
.674	.828				
.733	.845				
.691	.847				

[redacted]

[redacted]

TABLE III.- EXPERIMENTAL DATA FOR VARIABLE GEOMETRY; $\alpha = 2.1^{\circ}$ - Concluded

(c) $N_L C_i D_o{}' SG_{50}$

p_{t_2}/p_{t_∞}	m_3/m_∞	p_{t_2}/p_{t_∞}	m_3/m_∞	p_{t_2}/p_{t_∞}	m_3/m_∞
$M_\infty = 1.59$; $\delta_2 = 10^{\circ}$		$M_\infty = 1.59$; $\delta_2 = 13^{\circ}$		$M_\infty = 1.59$; $\delta_2 = 19^{\circ}$	
0.875	0.496	0.905	0.543	0.911	0.459
.935	.631	.961	.589	.956	.490
.957	.686	.953	.714	.959	.518
.940	.771	.940	.785	.958	.559
.928	.806	.934	.796	.953	.597
.902	.855	.924	.802	.949	.637
		.903	.812	.933	.668
		.947	.840	.911	.682
				.887	.692
				.832	.695
$M_\infty = 1.70$; $\delta_2 = 10^{\circ}$		$M_\infty = 1.70$; $\delta_2 = 13^{\circ}$		$M_\infty = 1.70$; $\delta_2 = 19^{\circ}$	
.810	.446	.894	.619	.880	.509
.890	.683	.947	.657	.945	.567
.938	.744	.940	.694	.942	.610
.910	.806	.935	.740	.938	.651
.891	.835	.931	.783	.933	.689
.883	.842	.912	.822	.910	.717
.857	.859	.873	.846	.872	.734
				.817	.748
$M_\infty = 1.90$; $\delta_2 = 10^{\circ}$		$M_\infty = 1.90$; $\delta_2 = 13^{\circ}$		$M_\infty = 1.90$; $\delta_2 = 19^{\circ}$	
.823	.781	.848	.725	.831	.612
.846	.829	.881	.758	.888	.660
.825	.834	.876	.787	.897	.692
.816	.838	.866	.812	.897	.713
.806	.877	.857	.836	.891	.736
.764	.879	.820	.857	.862	.809
		.778	.876	.837	.817
				.810	.818
$M_\infty = 2.00$; $\delta_2 = 10^{\circ}$		$M_\infty = 2.00$; $\delta_2 = 13^{\circ}$		$M_\infty = 2.00$; $\delta_2 = 19^{\circ}$	
.757	.790	.805	.776	.847	.731
.785	.843	.834	.822	.864	.759
.773	.865	.819	.835	.862	.772
.718	.894	.812	.862	.881	.808
.758	.898	.812	.862	.866	.829
		.776	.877	.831	.846
		.777	.879	.780	.856
		.731	.893		
				$M_\infty = 2.10$; $\delta_2 = 19^{\circ}$	
				.792	.745
				.824	.791
				.841	.827
				.820	.852
				.820	.854
				.784	.870
				.736	.878

[redacted]

[redacted]

A
2
1
4

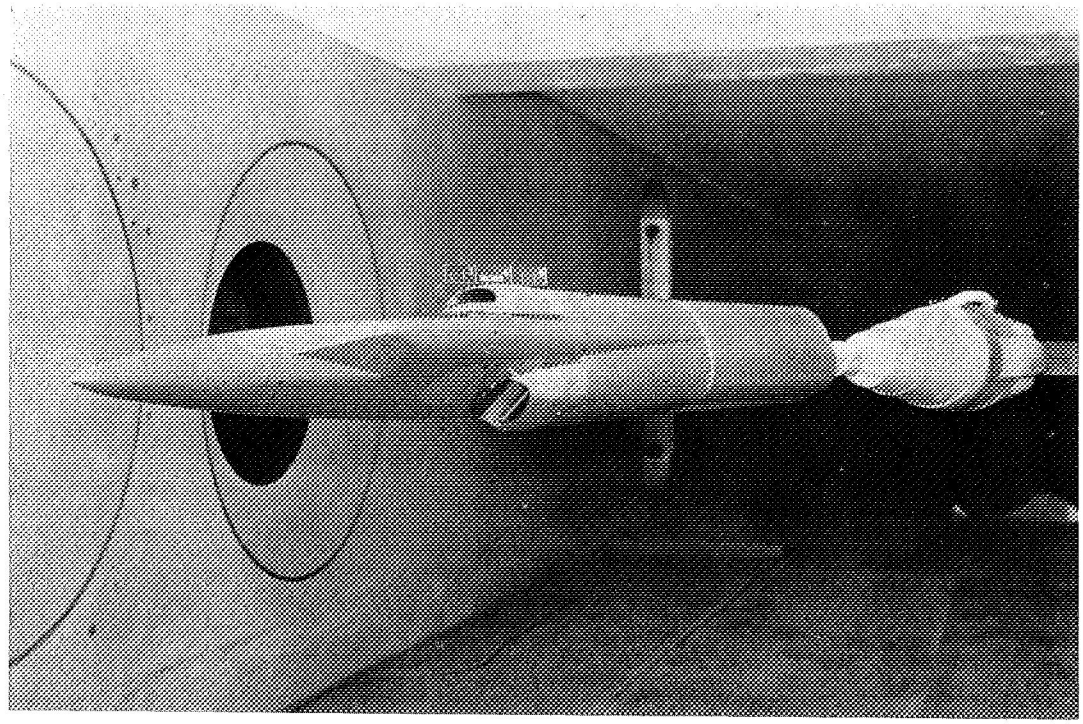

A-23146

(a) Typical configuration mounted in the wind tunnel.

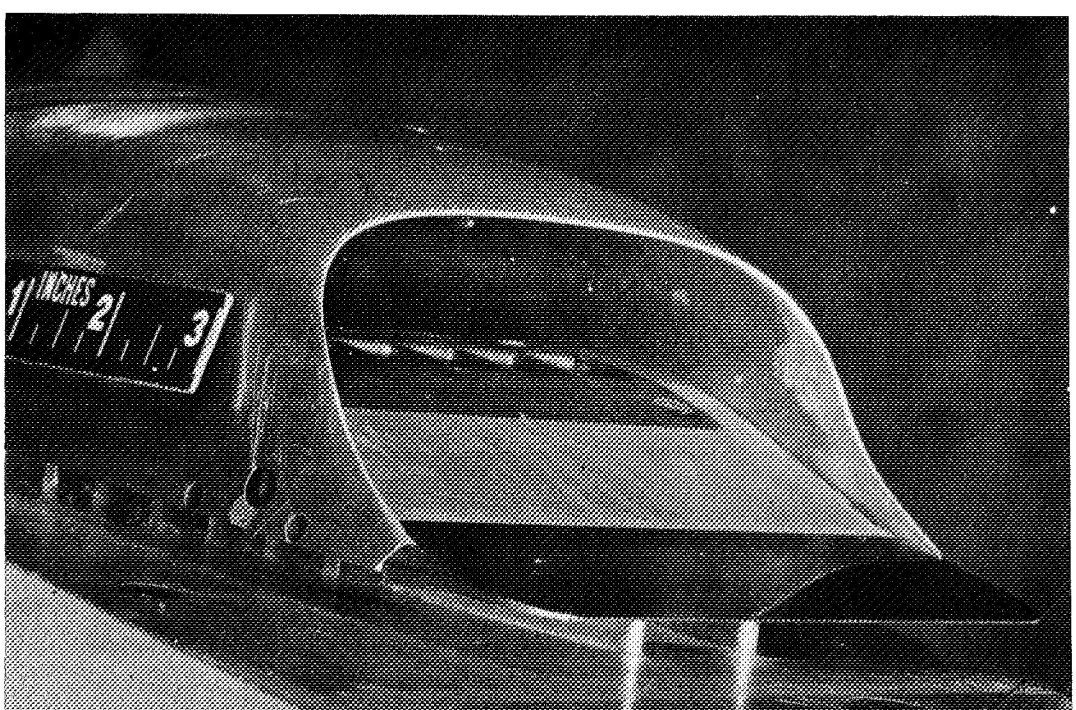

(b) Details of the inlet.

A-24088

Figure 1.- Photographs of the model.

[redacted]

[redacted]

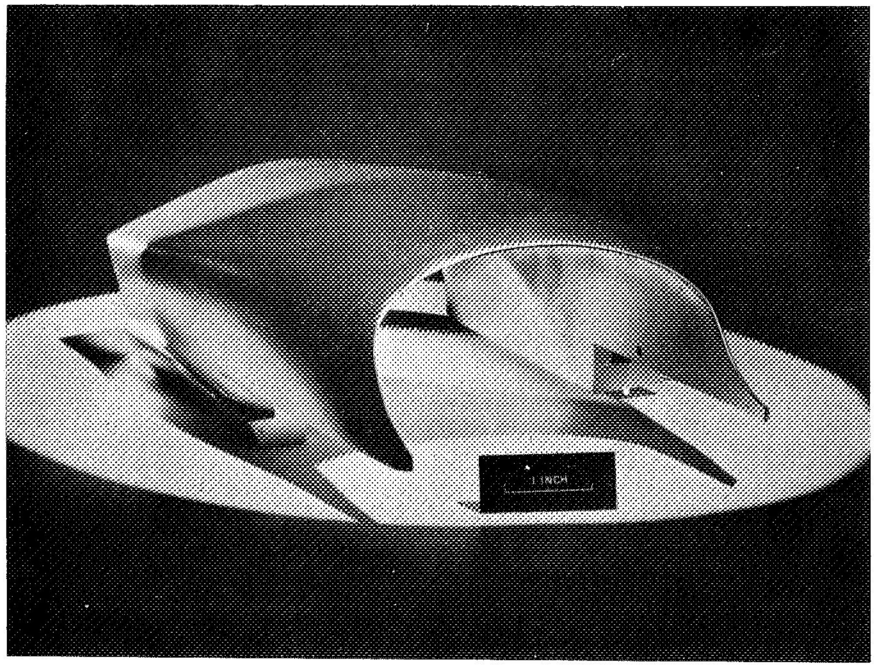

A-25743

(c) Original cowl, C_o.

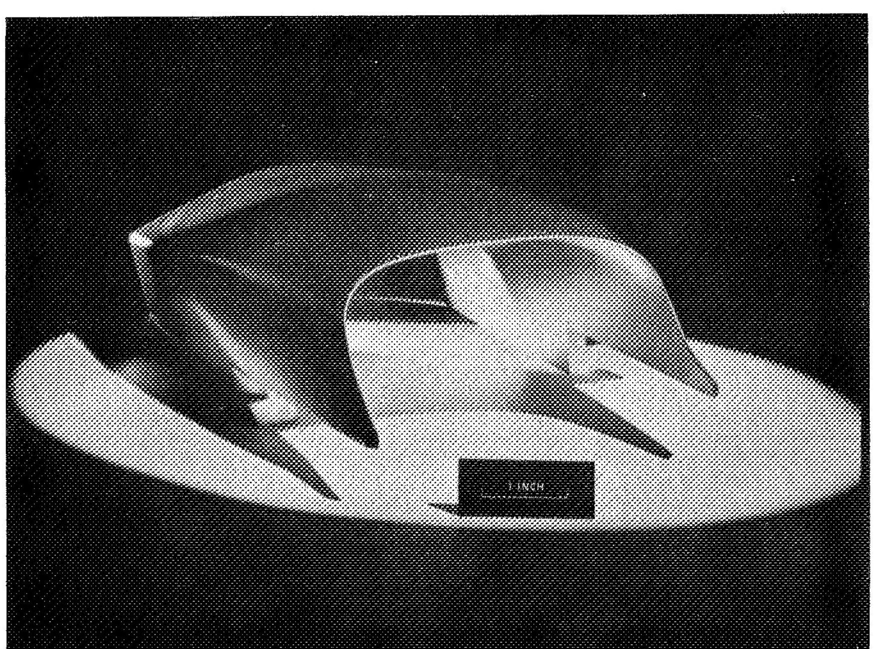

A-25744

(d) Modified cowl, C_o'.

Figure 1.- Concluded.

[redacted]

[redacted]

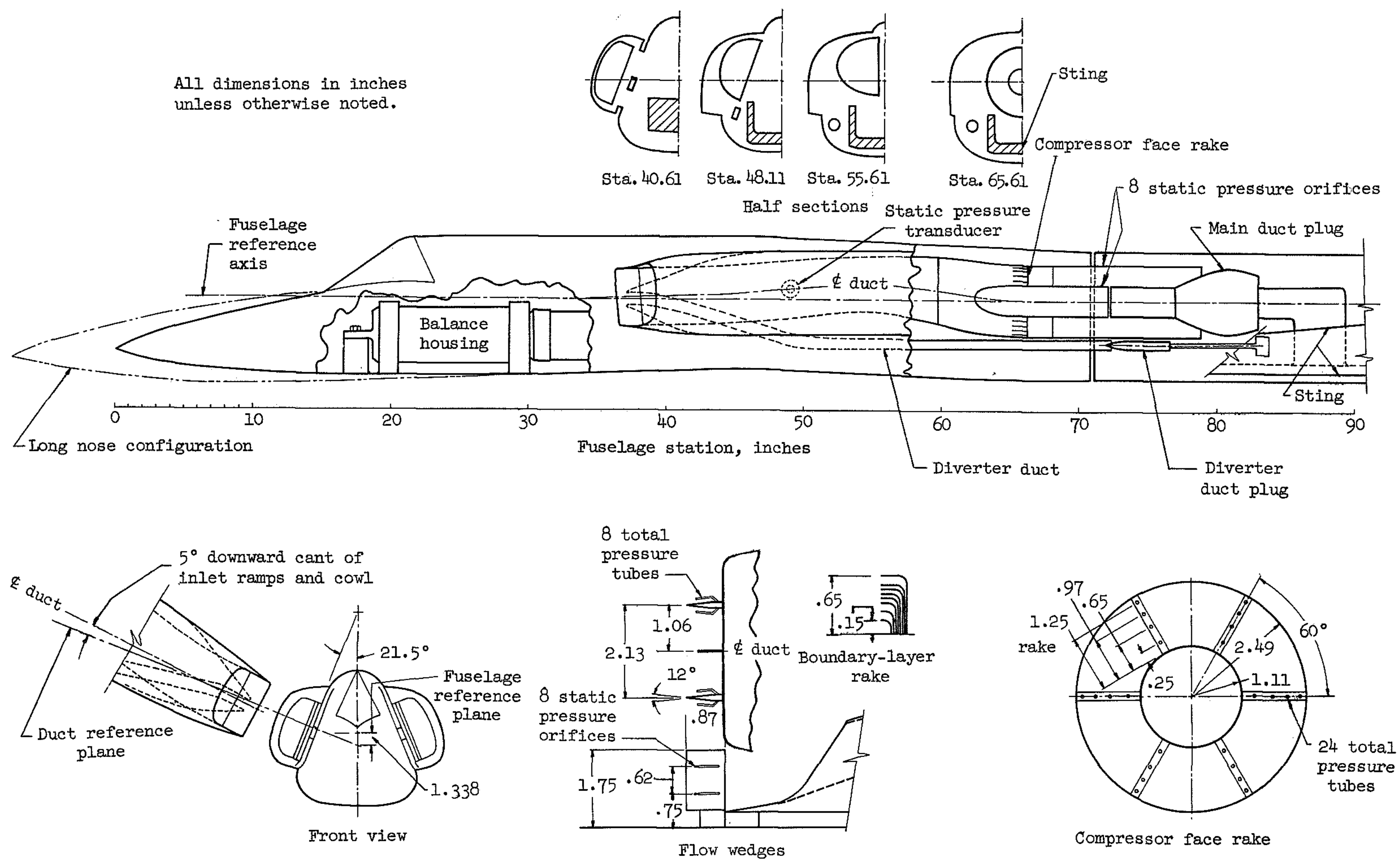

Figure 2.- Outline of the model and details of the instrumentation.

[redacted]

[redacted]

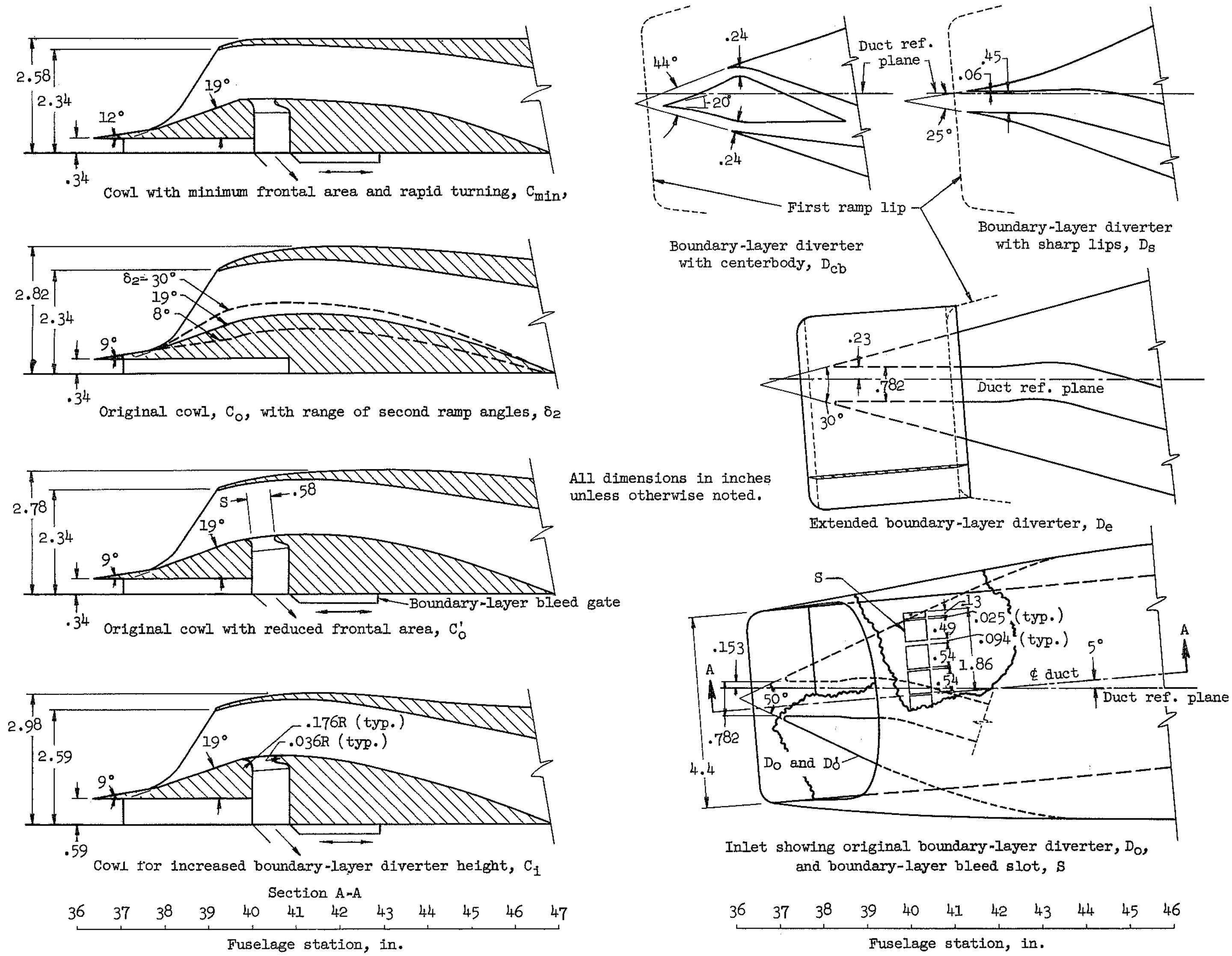

Figure 3.- Details of the cowls, bleed slot, and boundary-layer diverters.

[redacted]

[redacted]

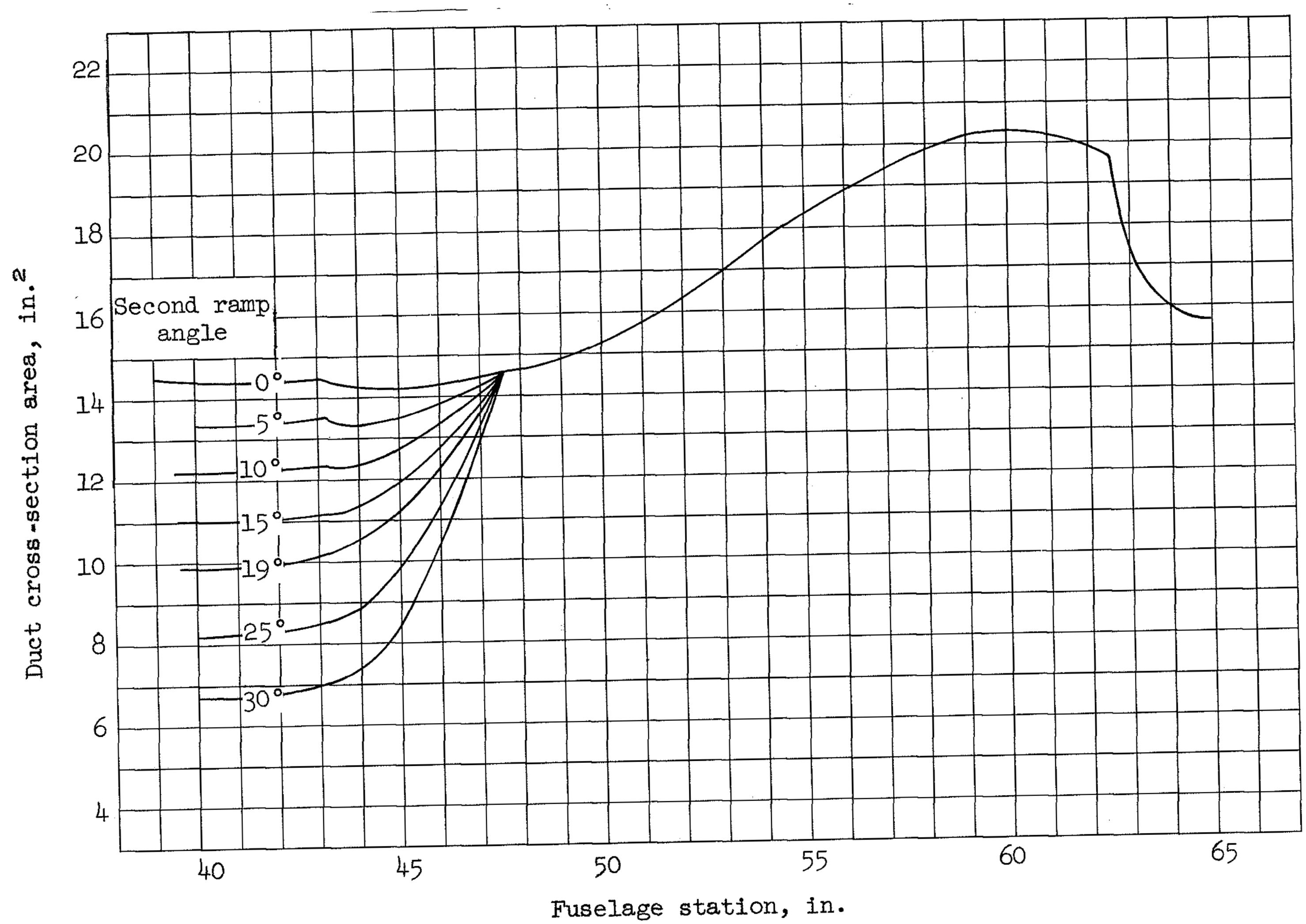

Figure 4.- Duct area distributions.

[redacted]

A
2
1
4

[redacted]

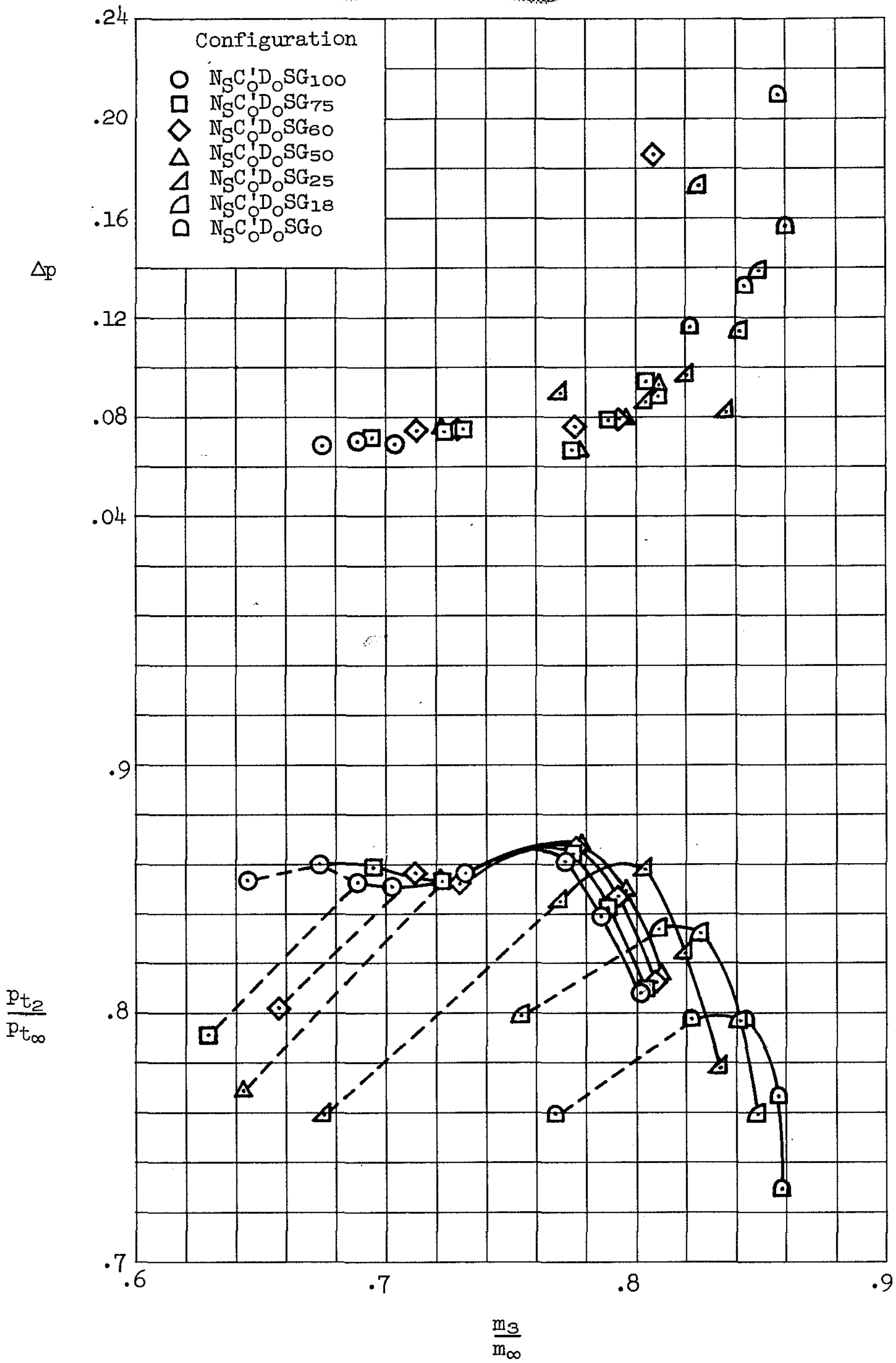

(a) Effect of bleed; short nose; $\alpha = 2.1^{\circ}$.

Figure 5.- Performance characteristics with boundary-layer bleed through the slot; $M_\infty = 2.00$.

A
2
1
4

[redacted]

[redacted]

A
2
1
4

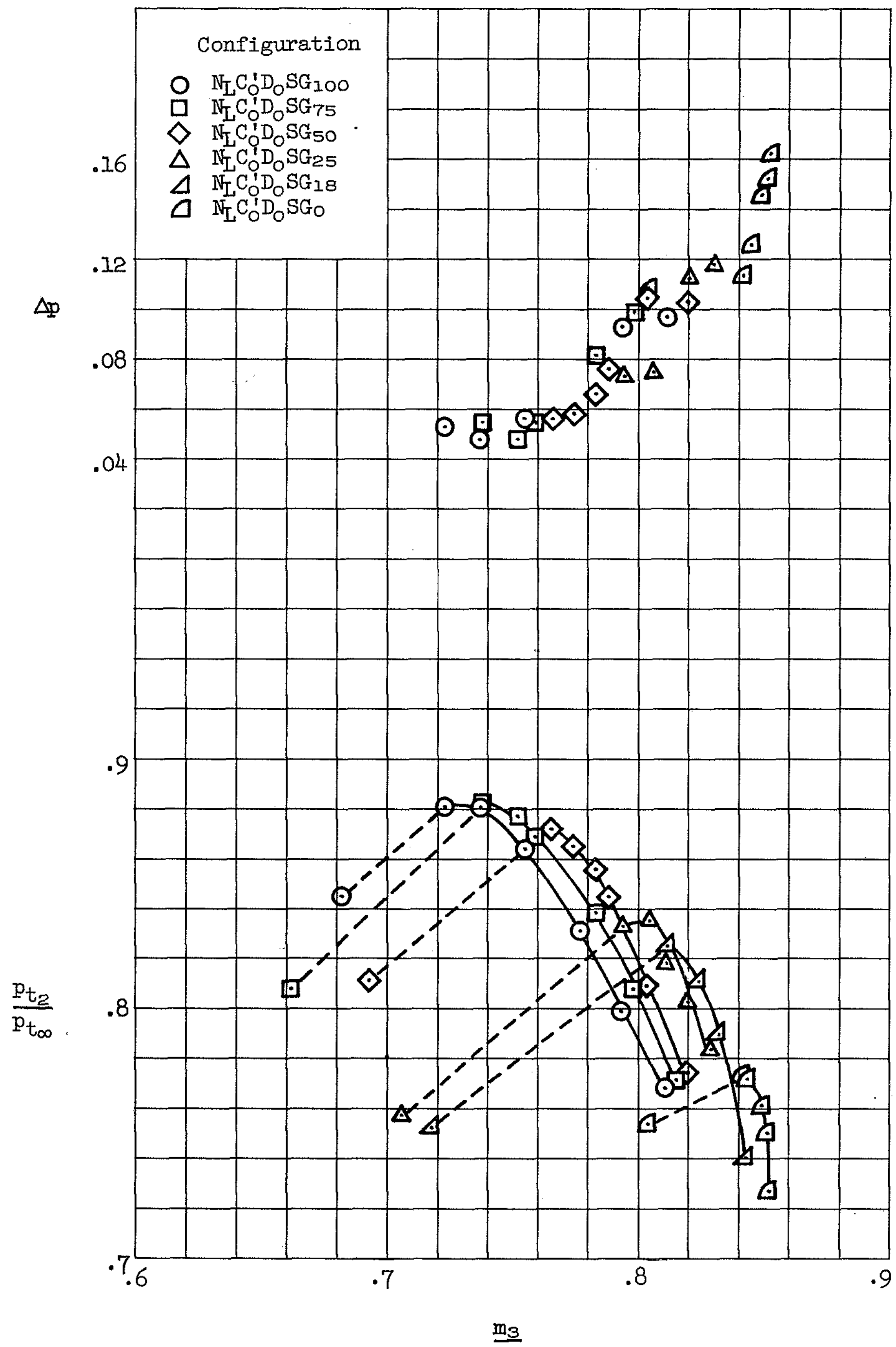

(b) Effect of bleed; long nose; α=2.1°.

Figure 5.- Continued.

[redacted]

[redacted]

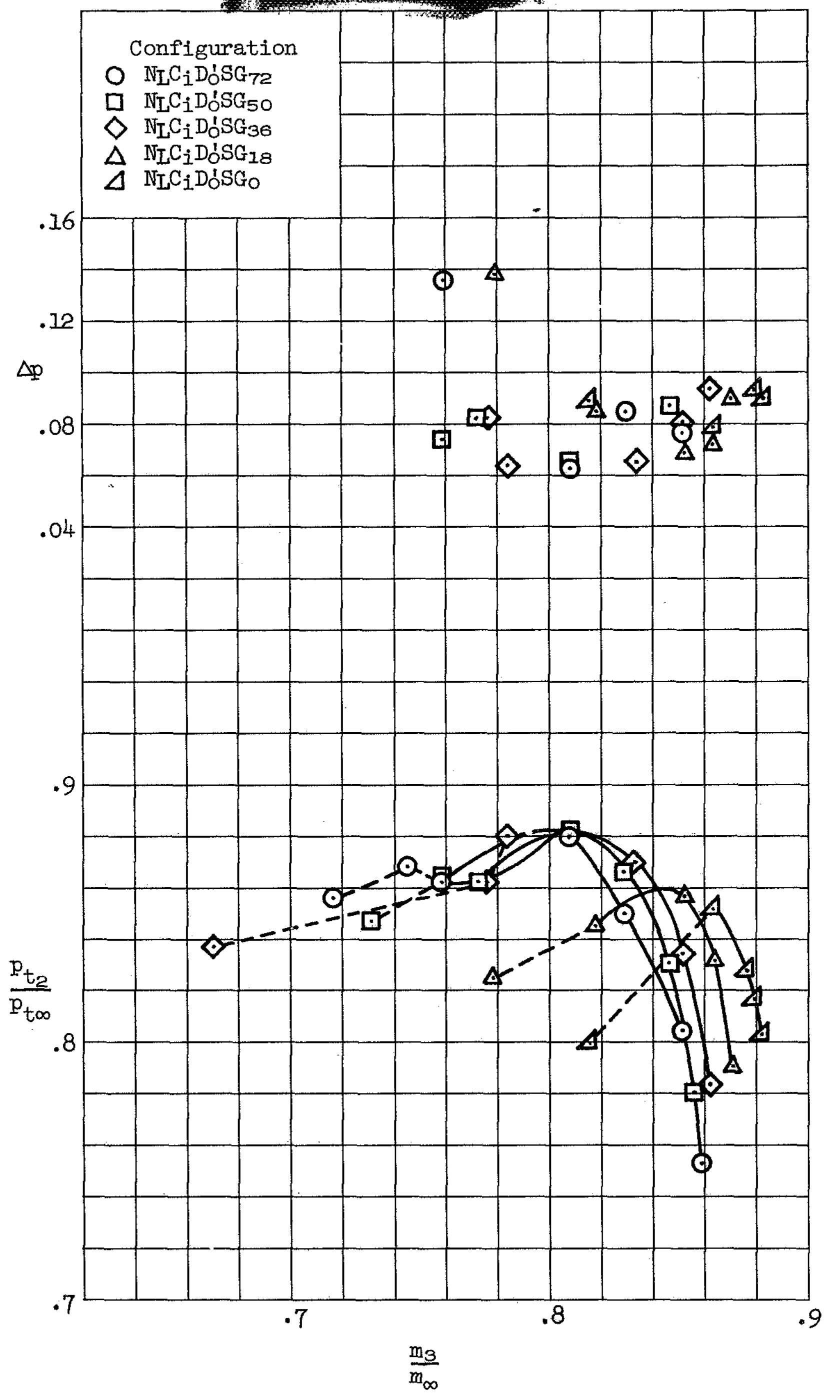

(c) **Effect of** bleed; long nose with the increased boundary-layer diverter height; $\alpha = 2.1^{\circ}$.

Figure 5.- Continued.

[redacted]

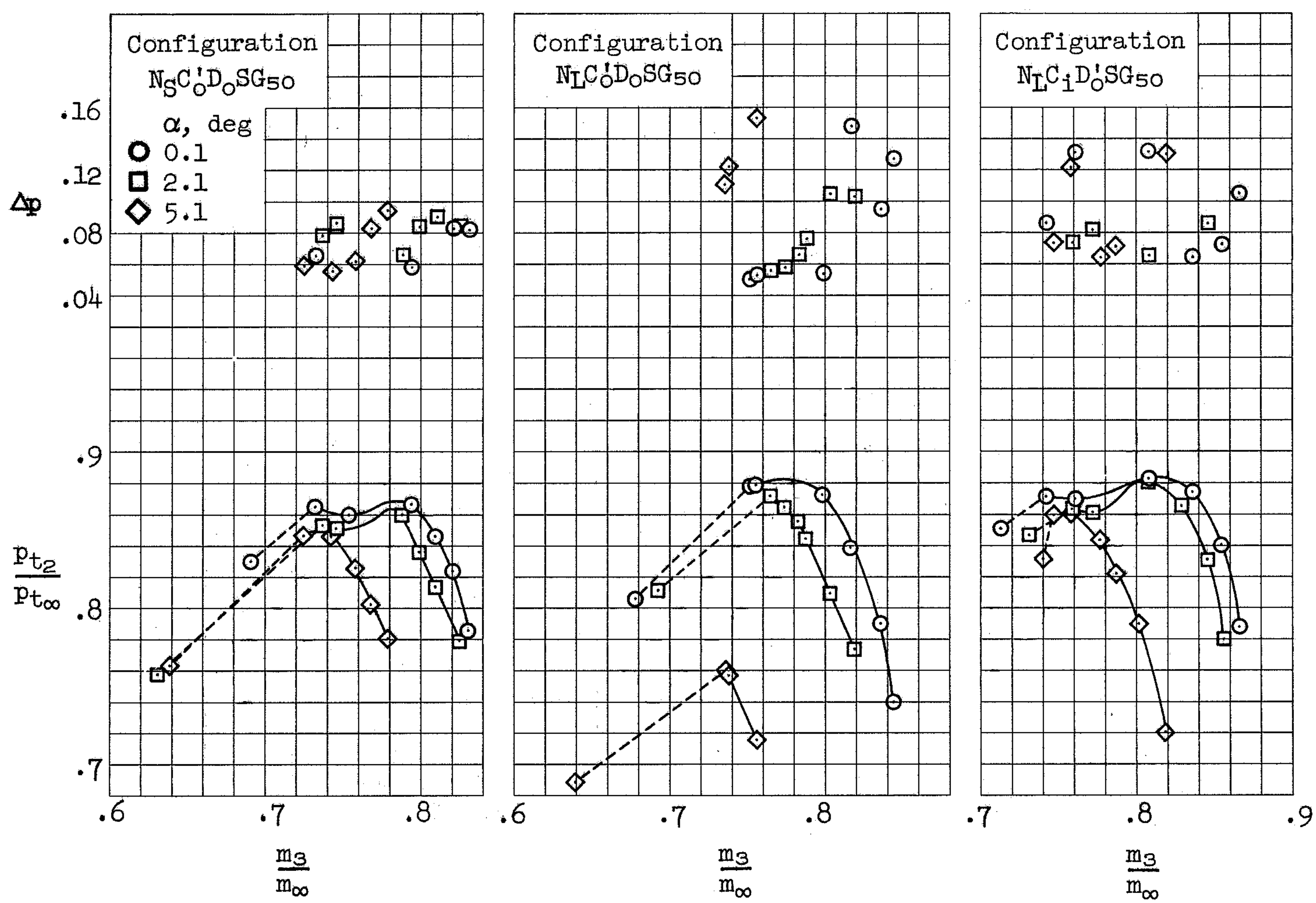

(d) Effect of angle of attack.

Figure 5.- Continued.

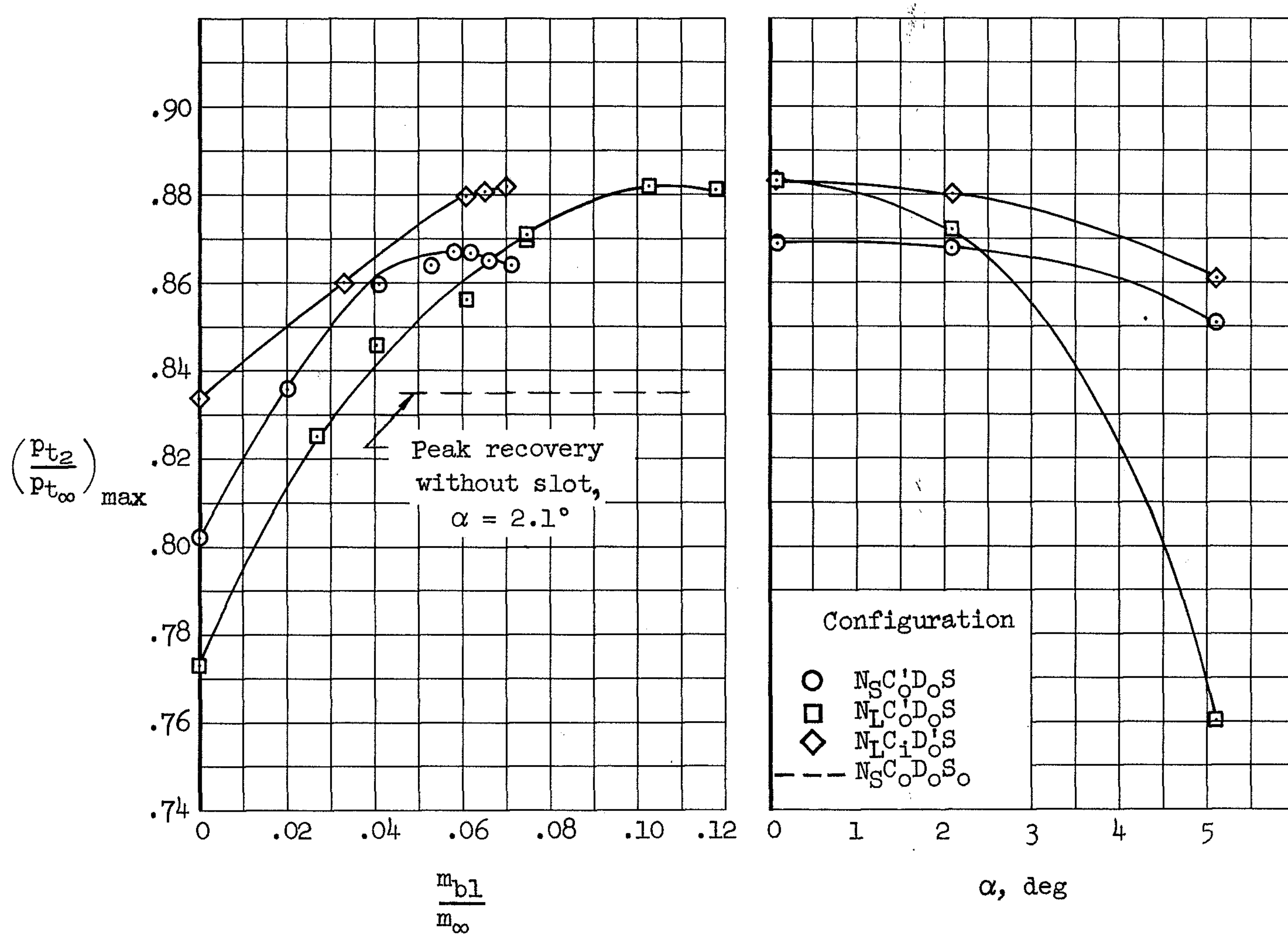

(e) Comparisons of maximum performance characteristics.

Figure 5.- Concluded.

A
2
1
4

[redacted]

A214

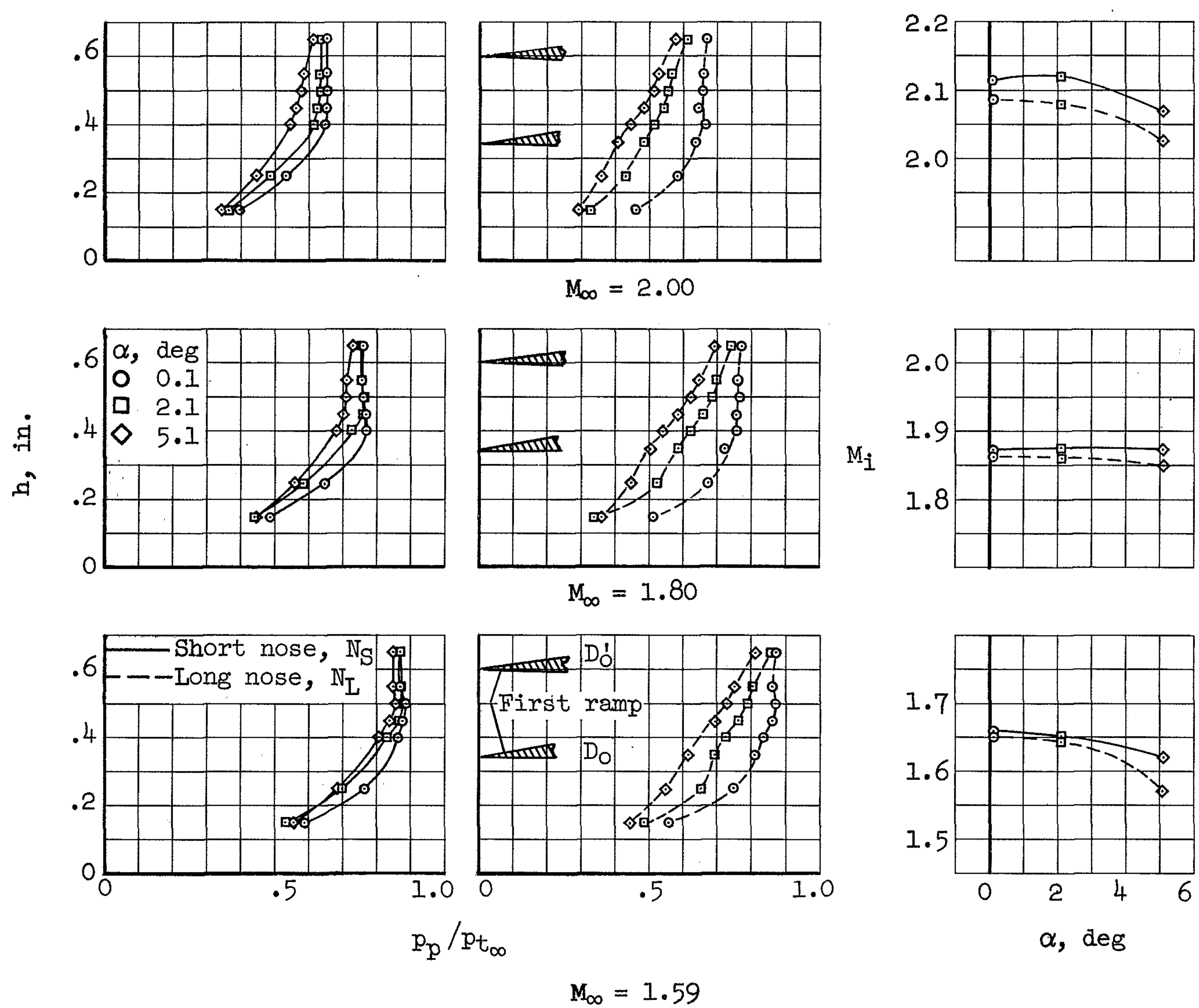

Figure 6.- Boundary-layer profiles and Mach number at the inlet.

[redacted]

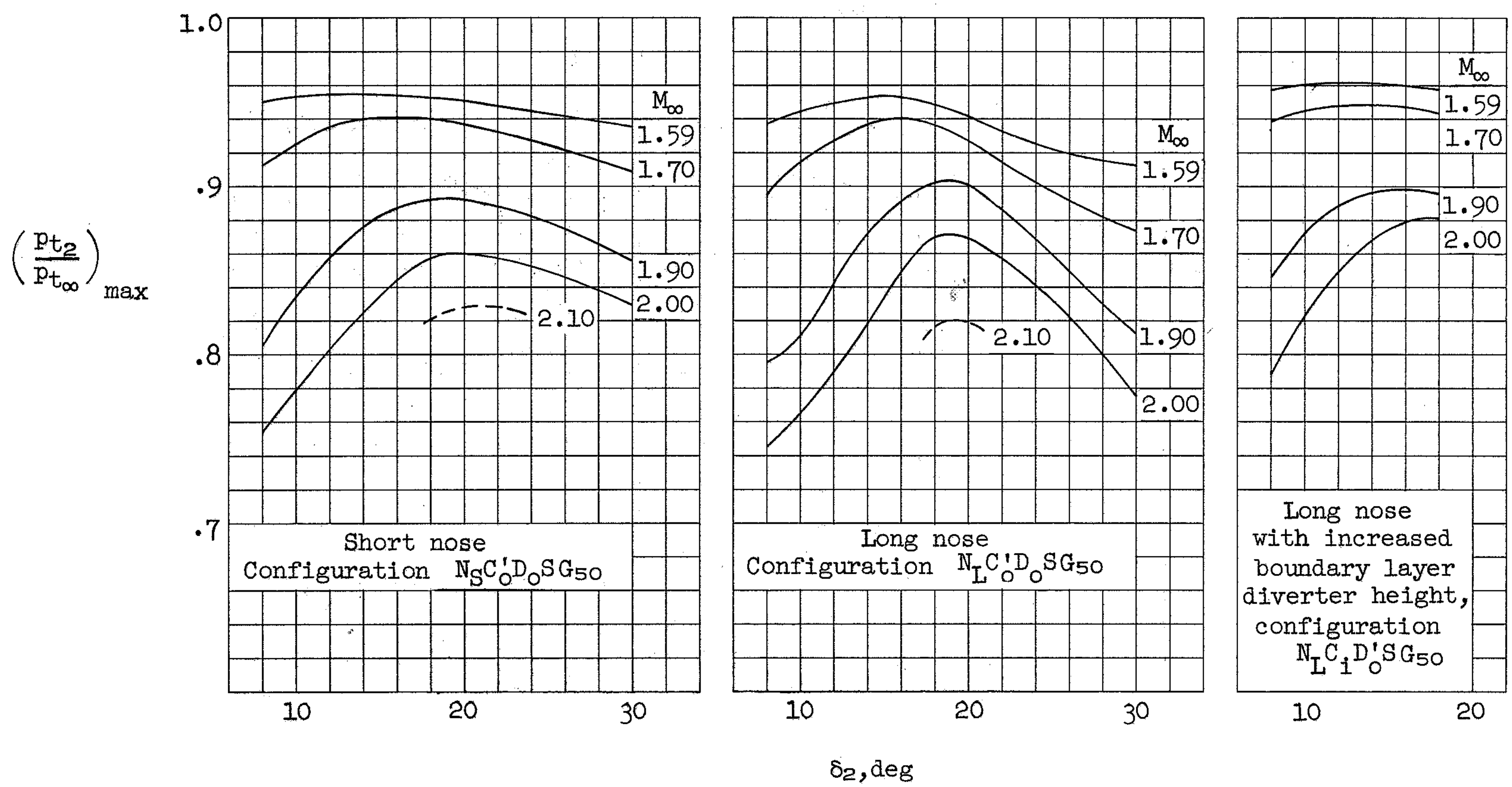

Figure 7.- Effect of variable geometry on the maximum total-pressure recovery; α=2.1°.

A214

[redacted]

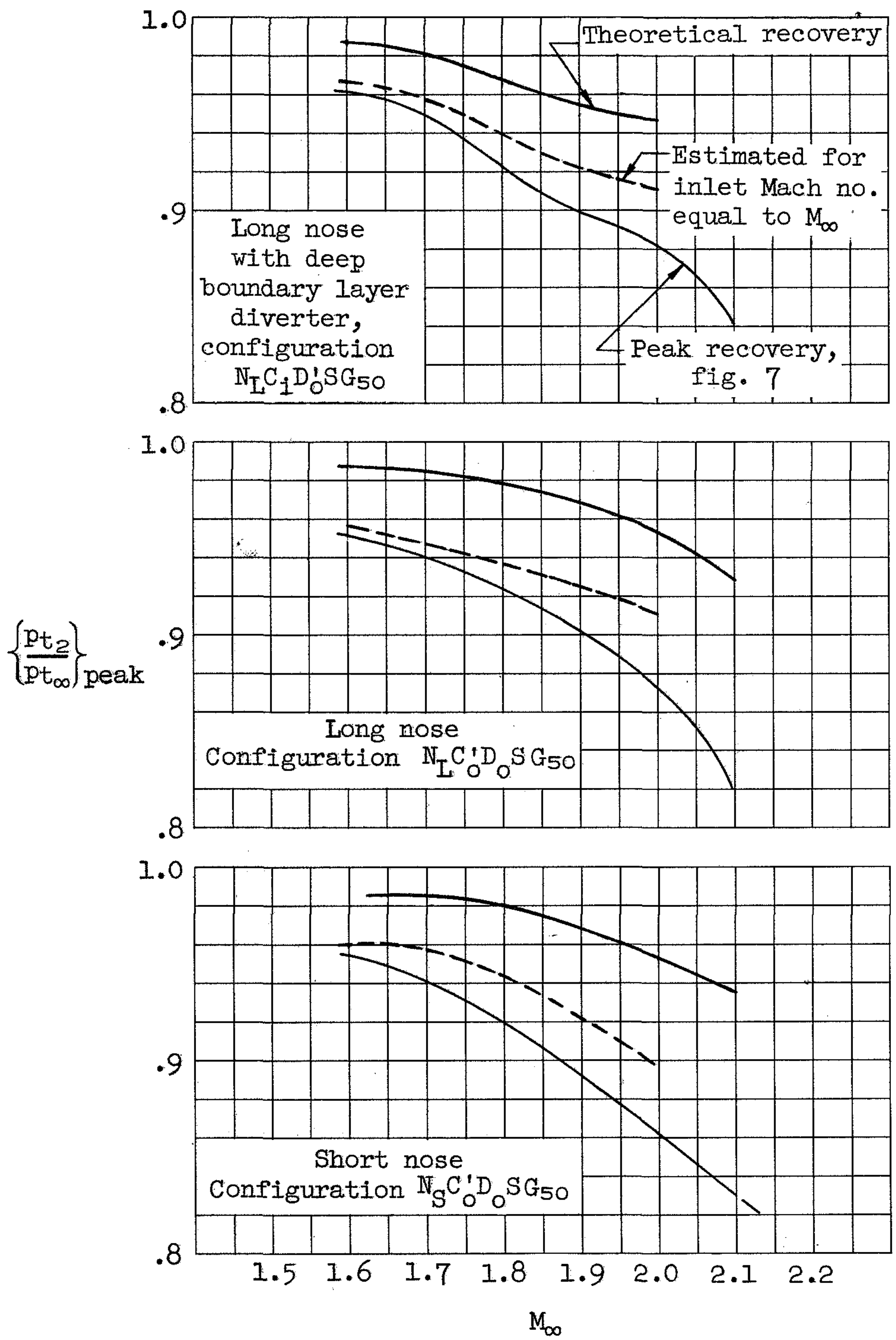

Figure 8.- Effect of fuselage flow field on peak total-pressure recovery; $\alpha = 2.1^\circ$.

[redacted]

[redacted]

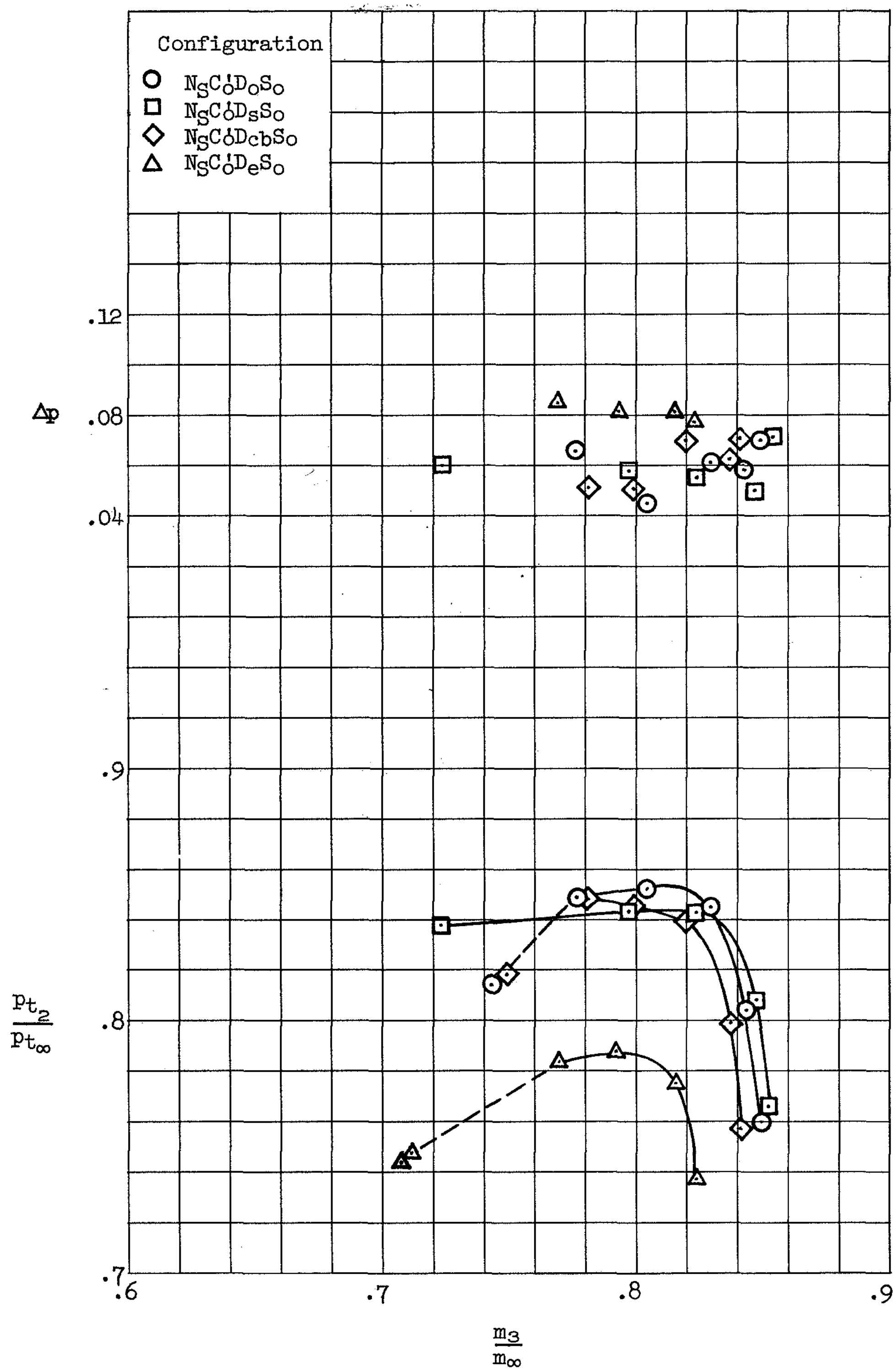

Figure 9.- Comparison of the performance characteristics with various boundary-layer diverters; $\alpha = 2.1^{\circ}$, $M_{\infty} = 2.00$.

[redacted]

[redacted]

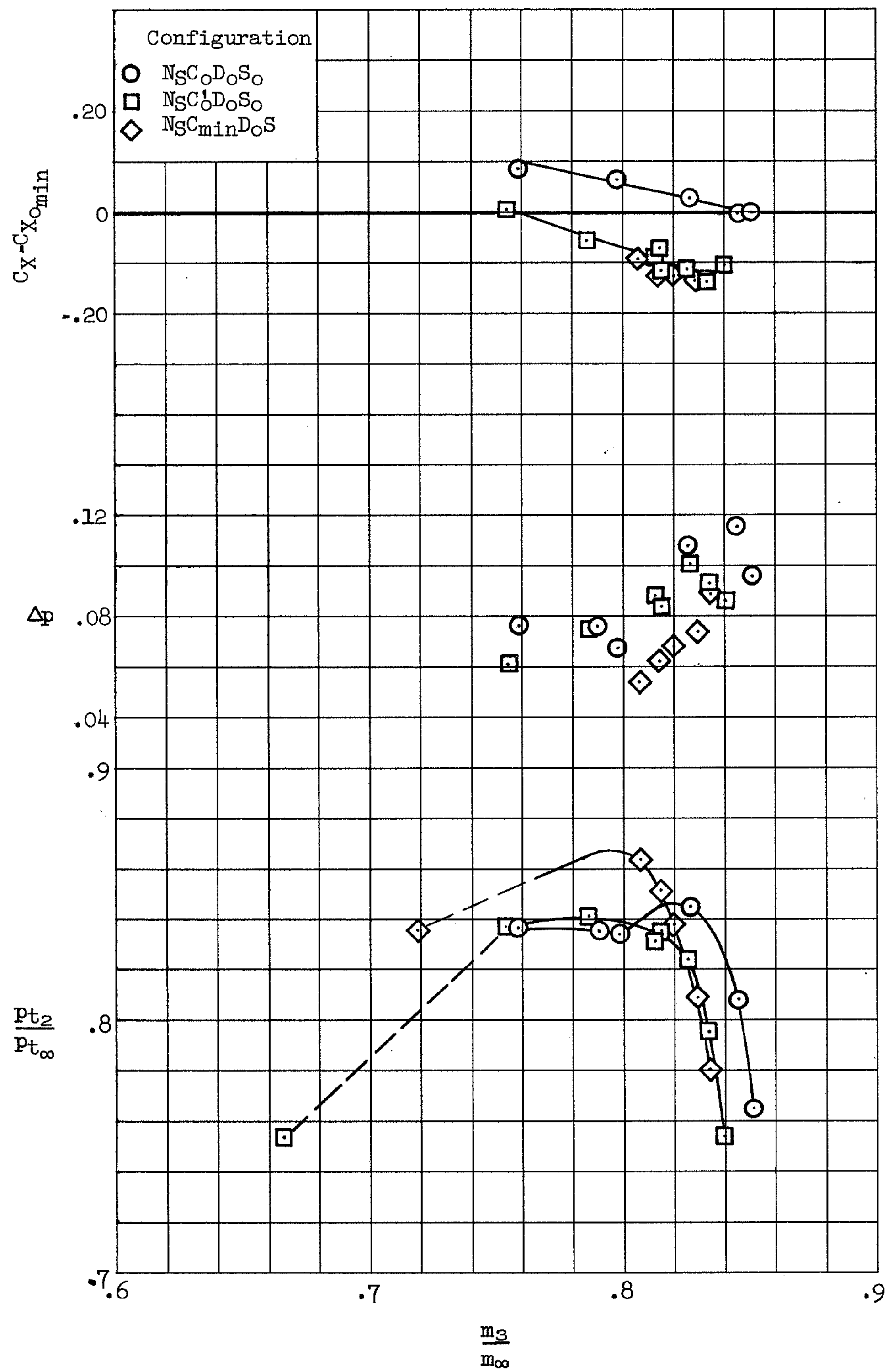

Figure 10.- Comparison of drag and performance for the various cowls; $\alpha = 2.1^{\circ}$, $M_\infty = 2.00$.

[redacted]

[redacted]

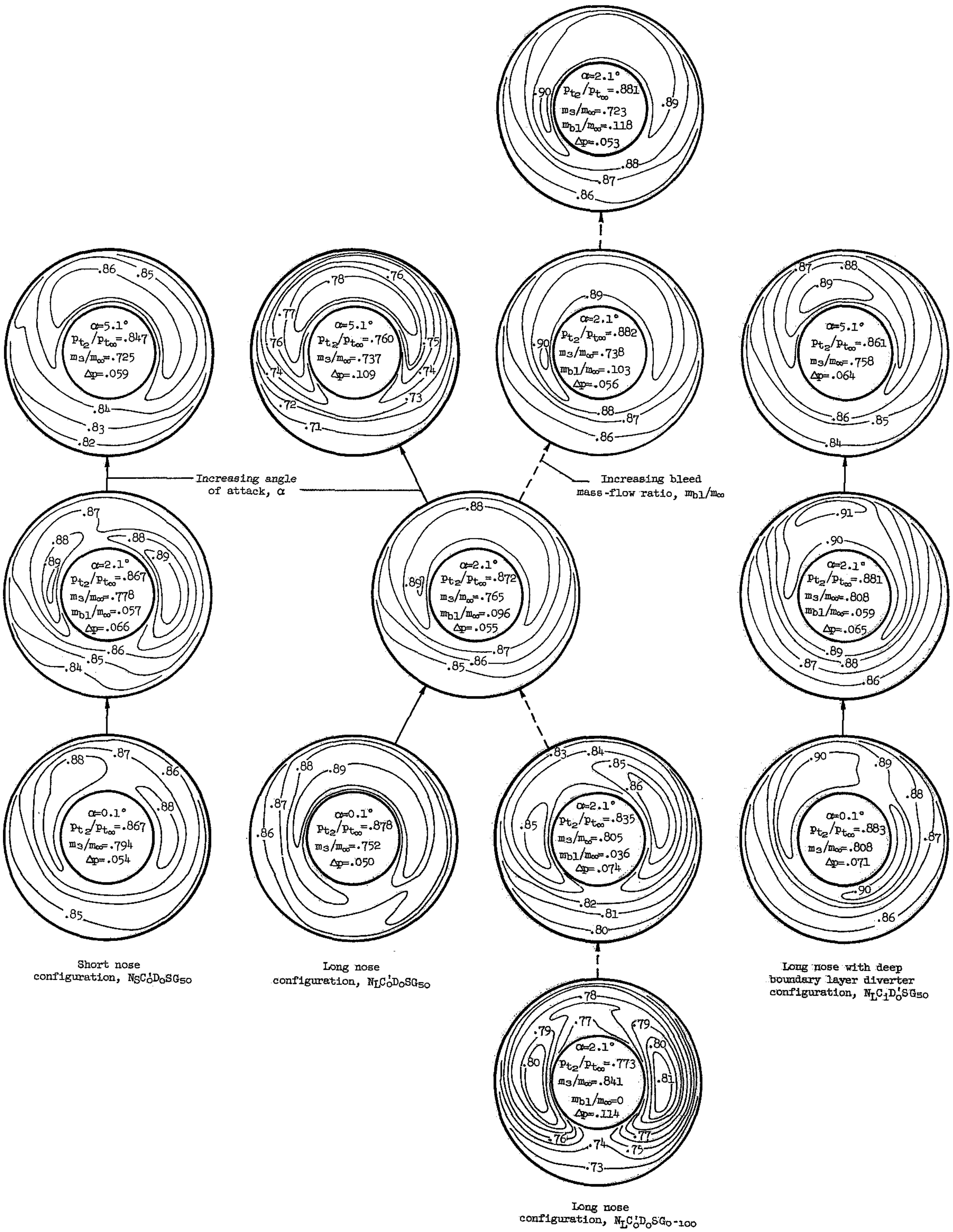

Figure 11.- Contours of total-pressure recovery at compressor face.

[redacted]

[redacted]

A214

NOTES: (1) Reynolds number is based on the diameter of a circle with the same area as that of the capture area of the inlet.

(2) The symbol * denotes the occurrence of buzz.

Report and facility	Description			Test parameters				Test data				Performance		Remarks
	Configuration	Number of oblique shocks	Type of boundary-layer control	Free-stream Mach number	Reynolds number × 10^{-6}	Angle of attack, deg	Angle of yaw, deg	Drag	Inlet-flow profile	Discharge-flow profile	Flow picture	Maximum total-pressure recovery	Mass-flow ratio[1]	
CONFIDENTIAL NASA TM X-163 AMES 9 by 7-Ft Unitary Plan Wind Tunnel	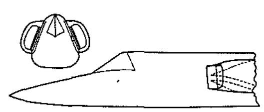	2 2 2 2 2	None Slot Bleed Slot Bleed Slot Bleed Slot Bleed	2.0 2.0 2.0 2.0 2.0	0.95 0.95 0.95 0.95 0.95	2.1 2.1 2.1 2.1 2.1	0.1 0.1 0.1 0.1 0.1	√ √				0.846 .867 .882 .882 .868	0.820 .777 .737 .805 .795 [1]Based on maximum inlet capture area	Short nose Short nose Long nose Long nose and deep plow Short nose and rapid turning of the internal flow
CONFIDENTIAL NASA TM X-163 AMES 9 by 7-Ft Unitary Plan Wind Tunnel	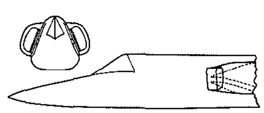	2 2 2 2 2	None Slot Bleed Slot Bleed Slot Bleed Slot Bleed	2.0 2.0 2.0 2.0 2.0	0.95 0.95 0.95 0.95 0.95	2.1 2.1 2.1 2.1 2.1	0.1 0.1 0.1 0.1 0.1	√ √				0.846 .867 .882 .882 .868	0.820 .777 .737 .805 .795 [1]Based on maximum inlet capture area	Short nose Short nose Long nose Long nose and deep plow Short nose and rapid turning of the internal flow
CONFIDENTIAL NASA TM X-163 AMES 9 by 7-Ft Unitary Plan Wind Tunnel	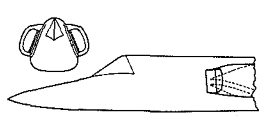	2 2 2 2 2	None Slot Bleed Slot Bleed Slot Bleed Slot Bleed	2.0 2.0 2.0 2.0 2.0	0.95 0.95 0.95 0.95 0.95	2.1 2.1 2.1 2.1 2.1	0.1 0.1 0.1 0.1 0.1	√ √				0.846 .867 .882 .882 .868	0.820 .777 .737 .805 .795 [1]Based on maximum inlet capture area	Short nose Short nose Long nose Long nose and deep plow Short nose and rapid turning of the internal flow
CONFIDENTIAL NASA TM X-163 AMES 9 by 7-Ft Unitary Plan Wind Tunnel	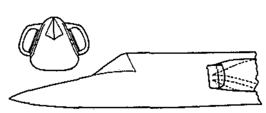	2 2 2 2 2	None Slot Bleed Slot Bleed Slot Bleed Slot Bleed	2.0 2.0 2.0 2.0 2.0	0.95 0.95 0.95 0.95 0.95	2.1 2.1 2.1 2.1 2.1	0.1 0.1 0.1 0.1 0.1	√ √				0.846 .867 .882 .882 .868	0.820 .777 .737 .805 .795 [1]Based on maximum inlet capture area	Short nose Short nose Long nose Long nose and deep plow Short nose and rapid turning of the internal flow

Bibliography

These strips are provided for the convenience of the reader and can be removed from this report to compile a bibliography of NASA inlet reports. This page is being added only to inlet reports and is on a trial basis.

[redacted]